Local Time–Temperature-dependent Deformation of a Woven Composite

by P. Shrotriya and N.R. Sottos

ABSTRACT—Moiré interferometry is utilized to investigate the time–temperature-dependent deformation of a woven composite substrate used in multilayer circuit board applications. Creep tests are performed at temperatures ranging from 27 to 70°C, and the resulting longitudinal and transverse displacement fields are measured via moiré interferometry. Measured displacement fields reveal the influence of fabric architecture on woven composite response. The deformation fields in the plane of the composite for loading along both warp and fill directions consist of a periodic arrangement of high-strain and low-strain regions in accordance to the interlacing bundle architecture. The deformation fields over the cross-section of the composite indicate that neighboring unit cells are subjected to equal and opposite bending moment even when the composite is loaded in uniaxial tension.

KEY WORDS—Woven composite, time–temperature-dependent response, Moiré interferometry, creep and stress relaxation, multilayer circuit boards, textile composites

Introduction

Multilayer printed circuit boards (PCBs) are used extensively in electronic packaging assemblies. The boards, shown schematically in Fig. 1, consist of multiple layers of woven glass/epoxy composite substrate sandwiched between copper foils. Significant residual stresses develop during processing and post-processing of multilayer boards due to mismatch of properties between the copper and woven composite layers. The residual stresses are large enough to cause such undesirable dimensional changes as warping and bowing of the boards and shrinkage of one layer with respect to the other. Board warpage and inner layer shrinkage cause problems with chip insertion, solder connection and interconnection between the layers and significantly affect the package reliability. Increases in circuit density make these problems even more severe as tolerance to dimensional changes is further reduced and the number of boards that pass quality standards decreases. The ability to accurately predict the residual stress state and to design dimensionally stable boards depends on accurate determination of the thermomechanical properties of the woven composite substrate.

P. Shrotriya (shrotriy@iastate.edu) and N.R. Sottos (SEM member), Department of Theoretical and Applied Mechanics, University of Illinois at Urbana-Champaign, Urbana, Illinois, USA. P. Shrotriya is currently at Mechanical Engineering Department, Iowa State University, 2025 Black Engineering Building, Ames, Iowa, USA.

Original manuscript submitted: February 11, 2002.
Final manuscript received: January 13, 2004.
DOI: 10.1177/0014485104044314

The composite substrate consists of an epoxy matrix reinforced by a plain weave fabric of glass fibers. A schematic diagram of the plain weave fabric is shown in Fig. 2. The fabric is composed of two sets of interlaced orthogonal warp and fill fiber bundles. A large number of plain weave fabric styles are currently used in circuit board design. The fabric styles are often unbalanced, i.e., the warp and fill directions include different numbers of fiber bundles or different sized fiber diameters. Because of the variation in fiber bundle sizes, the geometry of the undulating fiber bundles is different and depends on the fabric styles. Hence, composite substrates with different fabric styles have very different properties. Furthermore, the same fabric style has different properties in the warp and fill directions.

Sottos et al.[1] measured significant differences in the fabric geometry (bundle size, crimp, etc.), the elastic modulus, and coefficient of thermal expansion (CTE) in the warp and fill directions of two common substrates for multilayer circuit boards. Wu et al.[2] and Yuan and Falanga[3] characterized the CTE of substrates below the matrix glass transition temperature and detected higher CTE values in the fill direction. Wang et al.[4] generated master relaxation curves for a 109 style composite substrate and reported on different relaxation responses in the warp and fill directions. Shrotriya and Sottos[5] conducted experiments to characterize the fabric architecture and obtained different creep compliance curves in the warp and fill directions of a 7628 style composite substrate. During the processing and post-processing, the multilayer circuit boards are heated above the matrix glass transition temperature for an extended period of time. At temperatures near the glass transition, viscoelastic processes dominate the matrix response and result in time–temperature dependence of substrate properties. Shrotriya and Sottos[5] and Wang et al.[4] determined the global creep and relaxation response of woven substrates but there are no reported investigations on the influence of time–temperature-dependent matrix response on the local displacement field of a composite unit cell.

All of the studies described above suggest a strong influence of fabric architecture on the woven composite properties but the experimental measurements were performed at a length scale much larger than the composite unit cell. The woven composite was approximated as a homogeneous anisotropic continuum and the inhomogeneity of the unit cell (shown in Fig. 2) was ignored. The influence of the fabric architecture on the composite response is not studied directly. A detailed study of the local stress and displacement fields is required to fully understand the relation between the fabric architecture and woven composite response. A myriad of

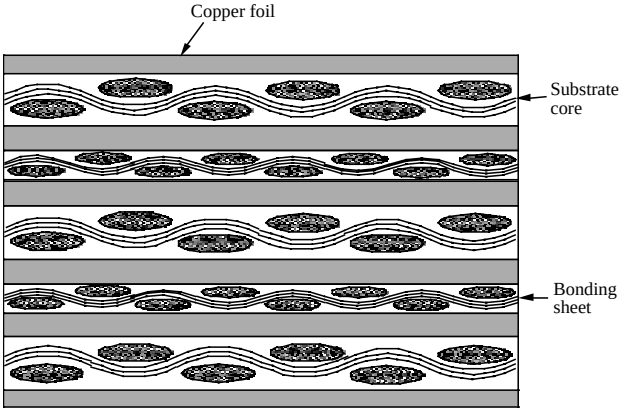

Fig. 1—Schematic diagram of a multilayer circuit board

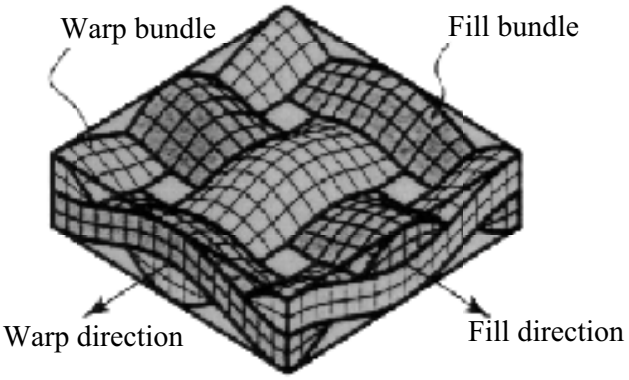

Fig. 2—Schematic diagram of a plain weave fabric

micromechanical models have been developed to predict woven composite response[6–8] but there are only a few reported experimental investigations of the local displacement fields.[9,10] The descriptions of the local fields are required to validate the physical basis of modeling assumptions and to understand the limitations of the models. Additionally, the local field descriptions may also be utilized to develop new micromechanical models for prediction of composite properties.

In this paper we describe a study of the local displacement field in a woven composite unit cell and its evolution with time and temperature. Moiré interferometry was utilized to investigate the deformation of the composite. Creep tests were performed at temperatures ranging from 27 to 70°C, and the resulting longitudinal and transverse displacement fields were measured via moiré interferometry. Moiré interferometry facilitates quantitative representation of the displacement fields and offers sufficient resolution ($\sim$0.42 μm) to conduct experiments at the length scale of the composite unit cell.[10] A number of researchers[9–11] have applied moiré interferometry for characterization of the textile composites. The current work focuses on the visualization and analysis of unit cell displacement during creep. Two different sample types are tested in order to investigate the creep deformation in the plane as well as in the cross-section of the reinforcing fabric. The displacement fields in the plane of the woven composite reveal the influence of fabric architecture on the inhomogeneity of deformation. The displacement fields in the cross-section are utilized to identify the deformation mechanism of the unit cell.

Experimental Apparatus and Test Procedure

A creep test apparatus was developed for use with a compact four-beam interferometer to test the composite specimens. The design of this apparatus, shown schematically in Fig. 3, was governed by the need to test the composite in two different configurations and over a range of temperatures. The compact interferometer requires the use of cross-line diffraction gratings with a virtual grating frequency f_V of 2400 lines mm^{-1}. Post et al.[10] provide a detailed description of the instrument. Samples were positioned within the 45 mm diameter viewing field of the compact four-beam interferometer using an x–y translation table, rotation stage, and screw adjustments on the interferometer. A pneumatic optical table isolated the entire assembly from ambient vibration. Moiré images were projected by the interferometer in the direction opposite from the creep testing machine and digitized using a high-resolution CCD camera and image acquisition software.

Creep Testing Apparatus

The portable dead-weight creep testing apparatus (shown in Fig. 3) was constructed from the pivoted crossbeam of a triple beam balance. The specimen was attached by pins to the two grips, one of which is suspended from an Stype load cell attached to the crossbeam. The specimen was loaded by placing mass on a pan hanging from the other end of the beam. The load carried by the specimen was measured using the load cell. The load cell could withstand a maximum load of 220 N and had a manufacturer's rated precision of $\pm$0.08 N. A temperature chamber designed to fit around the composite specimen[12] enabled creep tests at temperatures ranging from 23 to 80°C. Stout[12] designed the chamber for high-temperature testing of electronic components. The chamber is equipped with a flexible silicon rubber heater and is controlled by a PID controller with feedback provided by a thermocouple attached to the specimen. The chamber's primary insulation was semi-rigid 5 mm thick Pyropel board. A 5 mm thick Pyrex window provided optical access to the specimens. The limitations of enclosing loading fixtures while maintaining adequate space between the chamber window and optical elements of the interferometer restricted the geometry of the temperature chamber to a slim vertical profile. Moiré images at high temperatures showed no unsteady behavior as a result of air currents. Likewise, the introduction of the Pyrex window into the optical path of the laser beams did not have any influence on fringe patterns.[12]

Specimen Preparation

Two different types of specimens (shown in Figs. 4 and 5) were fabricated for creep testing. For the first type of specimen (Fig. 4), a diffraction grating was applied to the top surface of a rectangular (19 $\times$ 6.40 mm^2) woven composite strip using the technique described by Post et al.[10] The woven composite was obtained from commercially pressed boards following the procedure described by Shrotriya and Sottos.[5] The strip was mounted in specially designed gripping fixtures

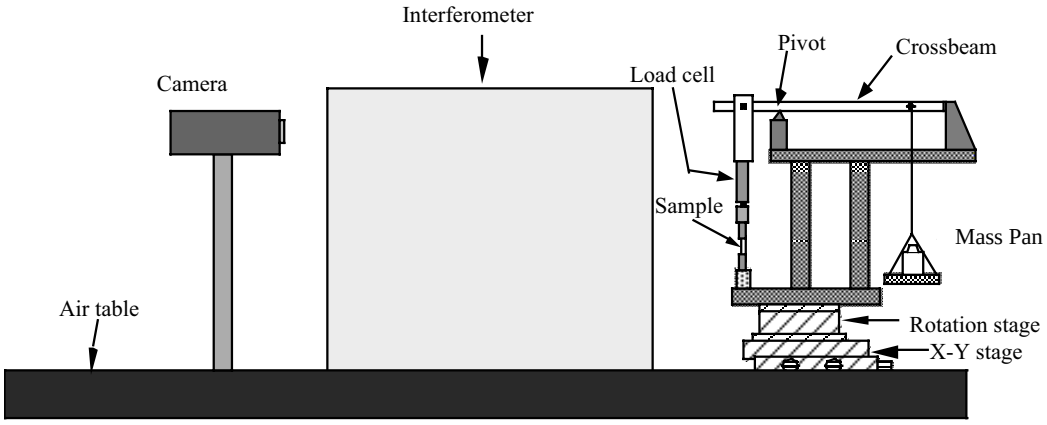

Fig. 3—Schematic diagram of the creep testing apparatus

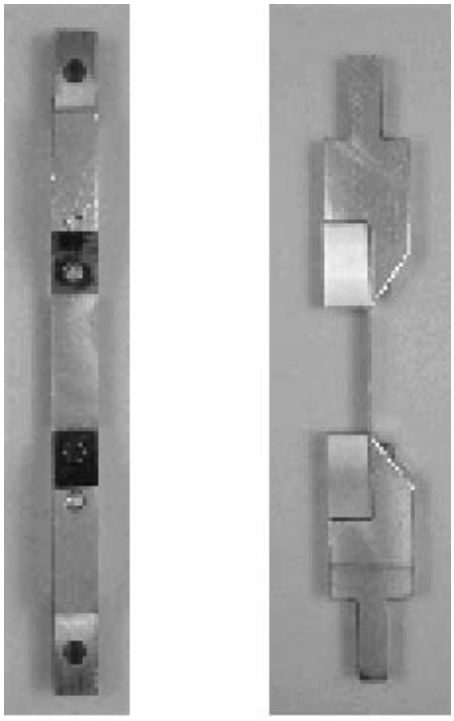

(a) (b)

Fig. 4—In-plane specimen: (a) front view; (b) side view

(a) (b)

Fig. 5—Edge specimen: (a) front view; (b) side view without the side supports

such that the surface with the diffraction grating faced the moiré interferometer. The fixtures were manufactured from stainless steel to minimize compliance and tapered such that the path of beams illuminating the diffraction grating is unhindered. This type of specimen was used to study the creep deformation in the plane of the composite and to understand the effect of bundle interlacing.

A second type of specimen (shown in Fig. 5) was prepared to investigate the creep deformation in the cross-section of the composite. Rectangular strips of the composite were cut in both the warp and the fill directions, and mounted in the specially designed fixtures such that the 0.17 mm thick cross-section of the composite faced the moiré interferometer. Two aluminum bars were attached on the sides of the fixtures to hold the specimen straight and to make handling easier. These bars were removed just before testing the specimen. The edges of the mounted composite strip were polished to ensure that the composite edges were planar with the fixture surfaces. The diffraction grating was applied to the surfaces of the fixture as well as the cross-section of the composite following the procedure outlined by Post et al.[10] If the diffraction grating had been applied only to the thin composite cross-section, the corresponding moiré image would

have been too small in size, making it difficult to align and locate the image. The combined moiré image of the composite cross-section and fixture surfaces was considerably larger and made the process of alignment easier.

Experimental Procedure

The creep tests were performed at four different temperatures ranging from 27 to 70°C. At each temperature, both the in-plane and the edge specimens were subjected to a constant load of 17.1 N for a period of 10 min, and 44 moiré images including the null field image were acquired over the entire time period. The acquisition times of the images were arranged such that the first 20 frames were acquired in the first minute of loading and the rest of the frames in the next 9 min. The creep tests were repeated twice at each temperature in order to record both U and V displacement fields. The creep load was within the linear response of the woven composite and sufficient time for full recovery of viscoelastic strains was allowed between successive creep tests for U and V displacement fields. Moreover, the in-plane specimens were also tested at three different load levels of 17.1, 26.2 and 34.0 N at room temperature, in order to determine the unrelaxed modulus and Poisson ratio of the composite.

The relation between fringe order and displacement is[10]

$$V = \frac{1}{f_v}\left(N_y + \frac{k}{\lambda}\right), \tag{1}$$

where f_v is the virtual grating frequency, which is chosen equal to $2f$, k is a constant, and N_y is the fringe order in the V field. The term $k\lambda/f_v$ is equivalent to a uniform displacement throughout the field, or a rigid body translation. For investigation of deformations, the rigid body motion is neglected, yielding

$$V = \frac{1}{f_v}N_y. \tag{2}$$

For characterization of more complex sample deformation, crossed line diffraction gratings are used in order to provide information about displacements U and V in the x- and y-direction, respectively. In practice, the crossed line grating allows pairs of incoming laser beams to produce fringe patterns of U and V deformation in succession either by using a four-beam interferometer or by rotating the sample by 90° when using a two-beam interferometer. The separate U and V field fringe patterns provide information about the displacement of every point in the images relative to every other point. The expression for the x-direction displacement is given by

$$U = \frac{1}{f_v}N_x, \tag{3}$$

where N_x denotes the fringe order in the U field.

For the analysis of moiré images, the partial derivatives in the strain equations were approximated by the ratio of the number of fringes along a line to the length of that line. The approximate versions of the strain equations are

$$\varepsilon_{yy} \approx \frac{1}{f_v}\frac{\Delta N_y}{\Delta y}, \tag{4}$$

$$\varepsilon_{xx} \approx \frac{1}{f_v}\frac{\Delta N_x}{\Delta x}, \tag{5}$$

$$\gamma_{xy} \approx \frac{1}{f_v}\left(\frac{\Delta N_y}{\Delta x} + \frac{\Delta N_x}{\Delta y}\right), \tag{6}$$

where ε_{xx} and ε_{yy} are the normal strain along the x- and y-direction, respectively, and γ_{xy} is the in-plane shear strain.

To obtain fringe counts along gage lengths, moiré fringe patterns were analyzed using an image processing software package following the procedure described by Stout.[12] The number of fringes in the moiré image corresponding to a null initial field were not sufficient to determine the variation of displacements over a unit cell. Instead, a carrier field of extension was utilized as the initial field in order to increase the number of fringes, and consequently to increase the resolution of displacement measurement.[10] Representative moiré images of a loaded surface specimen and the corresponding initial image with a carrier field of extension are shown in Fig. 6(a). The images were analyzed in order to provide the initial values for strain and displacement. All strains were calculated by subtracting the displacement in the initial field from the displacement in a final field to obtain the change in displacement across a gage length. Consequently, a single strain measurement required fringe counts from two different moiré images such that

$$\Delta N_i = N_{2i} - N_{1i}, \tag{7}$$

where $i = x$ or y. Depending upon the quality of the specimen and the fringe contrast of the image, fringe orders could be counted to within a quarter of a fringe.

In-Plane Creep Deformation

Moiré images obtained from loading the in-plane composite specimens at room temperature were analyzed in order to determine the unrelaxed (elastic) modulus and Poisson ratio along the warp and fill directions. A similar analysis was performed on images obtained from creep tests to determine the creep compliance at different temperatures. The composite properties calculated from analysis of the moiré fringes were compared with the previous experimental measurements reported in an earlier paper.[5] Unit cells of the fabric were identified by the periodic patterns of fringes acquired during testing. Fringes in a unit cell were analyzed to obtain a quantitative representation of the displacement and strain fields in order to determine the inhomogeneity caused by the interlacing bundle architecture.

Unrelaxed Modulus and Poisson Ratio

Moiré images corresponding to U and V displacement fields for a specimen along the fill and the warp directions were analyzed to determine the longitudinal and transverse strain at each load level by using eqs (4) and (5). As an illustration, the typical images corresponding to the warp direction are shown in Fig. 6. The unrelaxed modulus was determined using the best-fitting line of stress–strain curves for the fill and warp direction. Similarly, the Poisson ratio along the fill

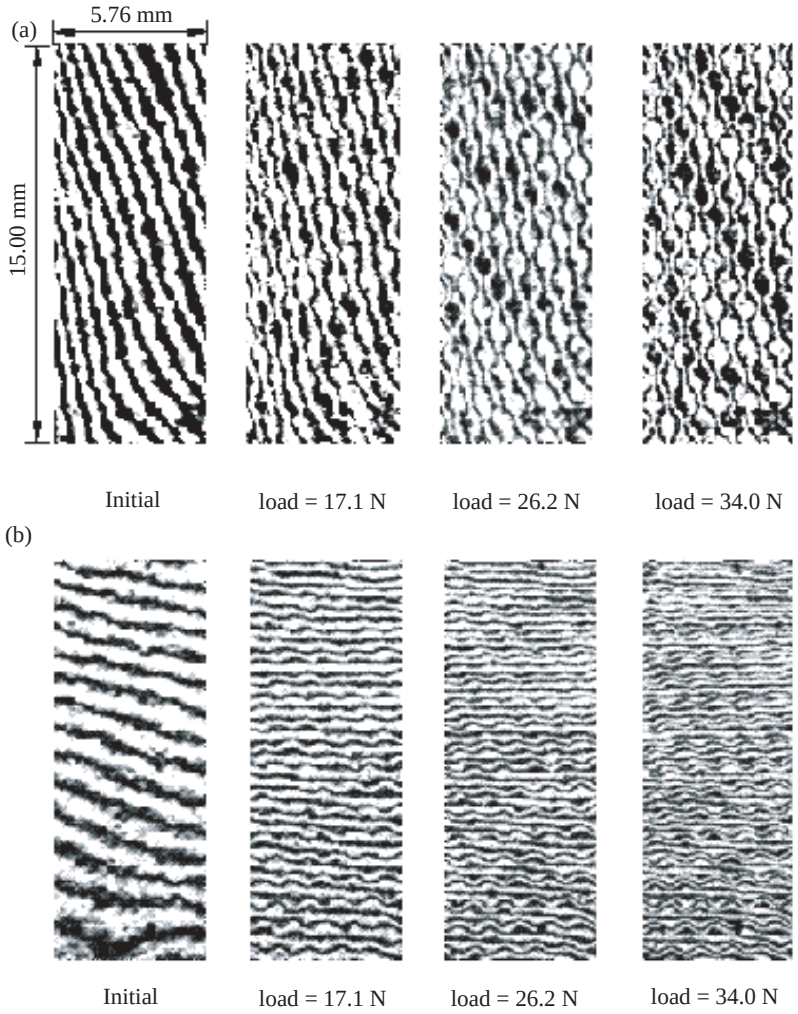

Fig. 6—Moiré images of the surface specimen along the warp direction at different load levels: (a) U direction field; (b) V direction field

TABLE 1—UNRELAXED MODULUS

Method	Fill (GPa)	Warp (GPa)
Moiré	21.4 ± 0.8	25.8 ± 0.8
Tensile test[5]	19.8 ± 0.5	24.5 ± 0.5

TABLE 2—POISSON RATIO

Direction	ν
Fill	0.26
Warp	0.21

and the warp directions was determined from the best-fitting line of transverse strain versus axial strain. The values of unrelaxed modulus determined from moiré images are compared with previously measured values[5] in Table 1. The values determined using the moiré analysis are slightly higher but within the experimental error of the previous measurements. The values determined for the Poisson ratio are presented in Table 2. The ratio of the Poisson ratio in the warp and the fill directions (ν_{xy}/ν_{yx}) is approximately equal to the ratio of the corresponding unrelaxed moduli (E_x/E_y) as required for an orthotropic material.

Creep Tests

Figure 7 presents sequences of moiré images corresponding to U and V displacement fields, obtained from the creep test of a composite specimen along the fill direction at a temperature of 27°C. Each sequence consists of initial images with a carrier of extension and images captured at different times after the application of load. For the sake of brevity, only two images from the sequence are presented in Fig. 7. Similar sequences were acquired for the creep tests of composite specimens along the fill and warp directions at temperatures of 27, 40, 60 and 70°C. The glass transition temperature (T_g)

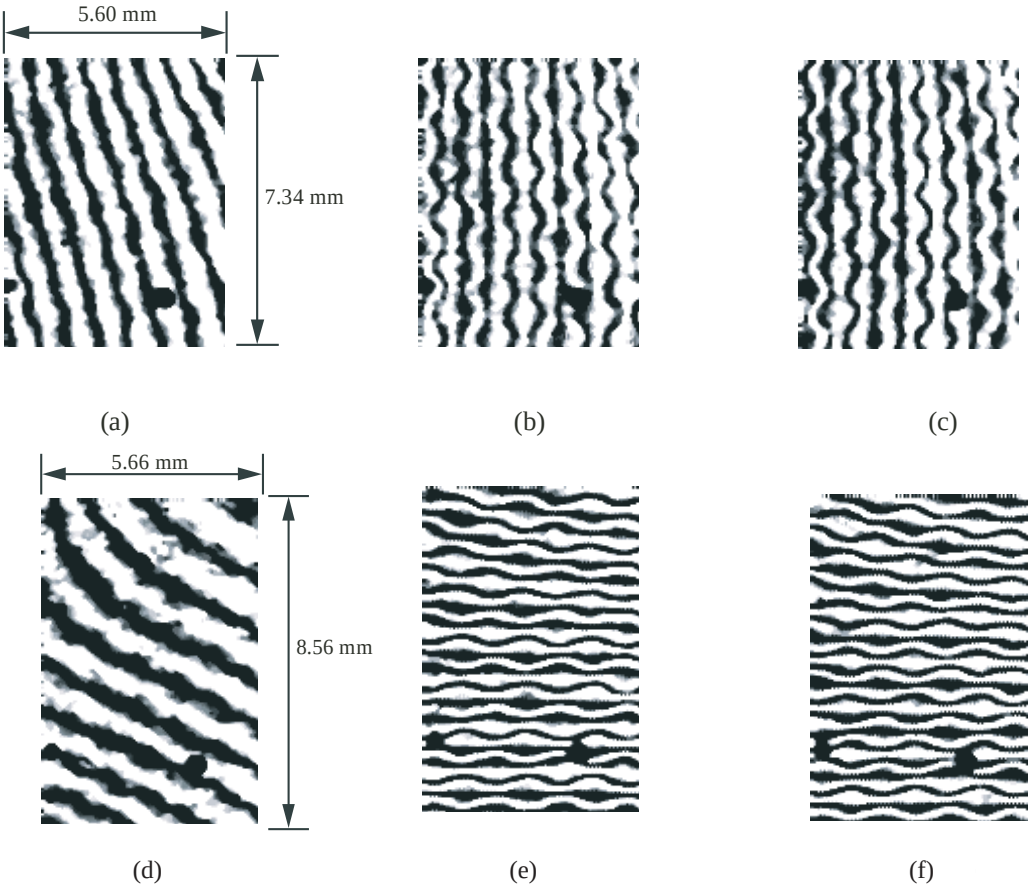

Fig. 7—Sequence of images corresponding to the creep test of a surface specimen along fill direction at 27°C: (a) initial U displacement field; (b) U displacement field at t = 8 s; (c) U displacement field at t = 600 s; (d) initial V displacement field; (e) V displacement field at t = 8 s; (f) V displacement field at t = 600 s

of the epoxy (Tra-Con F114) used to apply the diffraction grating is 53°C. The low T_g causes difficulties in acquiring moiré images above 70°C because of the viscoelastic relaxation of the epoxy. The V displacement images were analyzed in order to determine the creep compliance of the composite at each temperature. The analysis of moiré images reveals that the composite undergoes minimal creep deformation over the time range of the experiments. In addition, the uncertainty of half fringe order associated with counting of fringes further limits the sensitivity of the strain values calculated from the moiré images. Creep compliance of the composite at time = 10 min is plotted as a function of temperature for loading along both fill and warp directions in Fig. 8.

Unit Cell Displacement Field

Moiré images corresponding to U and V displacement fields of specimens shown in Figs. 6 and 7 consist of periodically repeating patterns of alternating high and low fringe density regions, corresponding to the architecture of plain weave fabric. In the tensile V displacement field, fringe density (strain) is highest in the regions where the fibers aligned to the x-direction (transverse) are closest to the surface, and the fringe density is lowest in the regions where the fibers aligned to the y-direction (loading) are closest to the surface. Similarly, regarding the negative U displacement field, fringe density is highest in the regions where the fibers aligned to the y-direction (loading) are closest to surface, and fringe density is lowest in the regions where the fibers aligned to the x-direction (transverse) are closest to the surface.

The smallest repeating unit of the image was identified for specimens along both fill and warp directions. As an illustration, a repeating unit is depicted in the moiré images corresponding to V and U displacements for the fill direction in Figs. 9(a) and (b), respectively. The repeating unit corresponds to four symmetrically arranged composite unit cells, as shown in Fig. 9(c). Fringe distribution over the repeating unit was monitored in creep tests performed at different temperatures. During a creep test the fringe distribution remained nearly constant. Therefore, only one representative moiré image was analyzed in order to obtain quantitative representation of the displacement fields at each temperature.

In each moiré image of the repeating unit, centerlines of the black fringes were located and fringe orders were assigned by arbitrarily choosing the zero-order fringe. The displacement field was determined by assuming a linear interpolation between the centerlines of the black fringes. Similar analysis was performed on the initial image in order to calculate the field corresponding to the carrier fringes. The initial field was subtracted from the calculated displacement field in

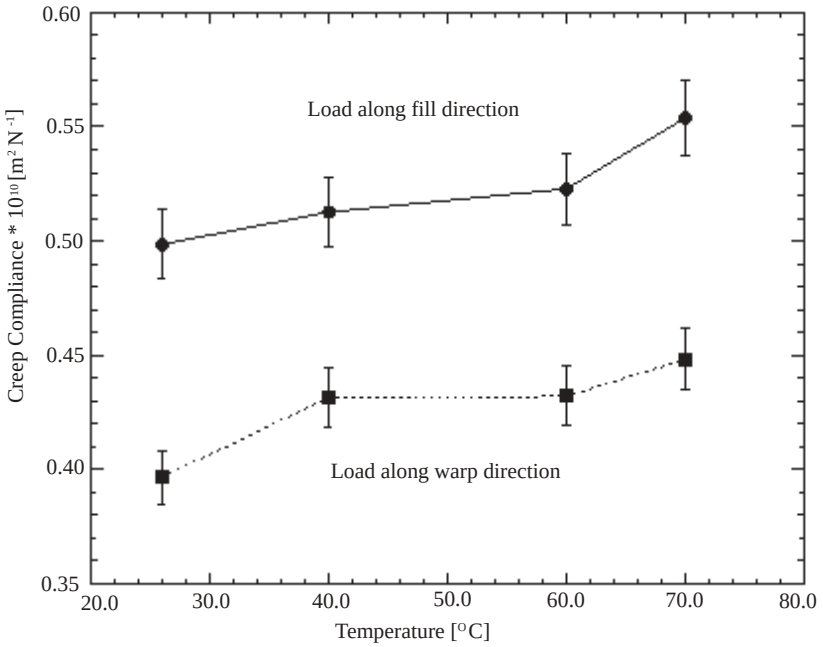

Fig. 8—Creep compliance of the composite at t = 600 s, determined from moiré images as a function of temperature

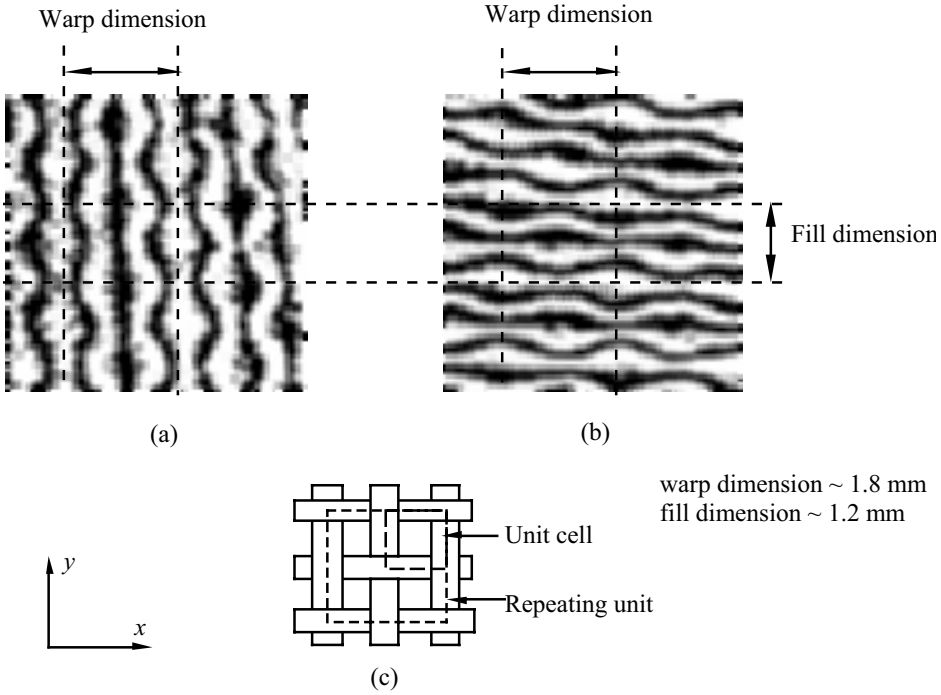

Fig. 9—Repeating unit of the moiré images: (a) U displacement at 27°C; (b) V displacement at 27°C; (c) schematic diagram of fabric architecture

order to determine the deformation of the repeating unit. As an illustration, Fig. 10 presents contour plots of the V and U deformation of the repeating unit loaded along the fill direction for 27 and 70°C.

As seen in the contour plots corresponding to the fill direction loading, the V displacement field at a given temperature (Figs. 10(a) and (c)) shows a local spatial variation but the total V deformation over the repeating unit (the difference between the top and bottom of the repeating unit) is nearly constant for any line drawn parallel to the loading direction. Similarly, the total U deformation (Figs. 10(b) and (d)) at a given temperature is nearly

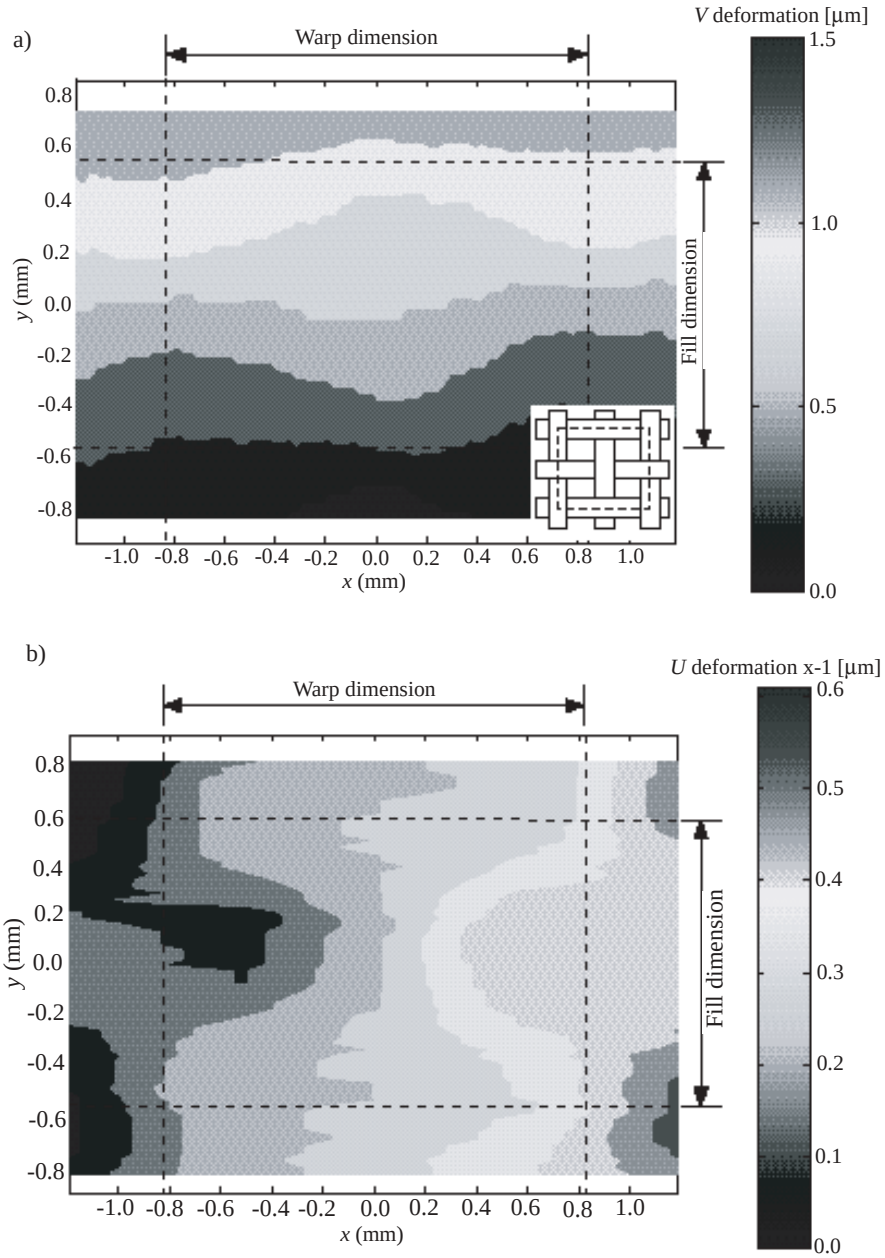

Fig. 10—Contour plot of displacement fields for the repeating unit loaded along fill direction: (a) *V* deformation at 27°C (architecture of repeating unit in the inset); (b) *U* deformation at 27°C; (c) *V* deformation at 70°C; (d) *U* deformation at 70°C
(Continued on next page)

constant for any line drawn perpendicular to the loading direction. Additionally, the *V* and *U* deformations are symmetric about the centerlines of the repeating unit. The symmetry of the deformation follows from the symmetric architecture of the repeating unit.

The architecture of the repeating unit (Fig. 9(c)) is such that fibers aligned to the fill direction are closest to the surface in the center and at the four corners. As a result, in the center and at the corners of the repeating unit, the contours corresponding to *V* deformation are spaced further apart, indicating a region of low tensile strain, whereas the contours are clustered together at the mid-points of the sides, indicating a region of high tensile strain. The contours corresponding to the negative *U* deformation are clustered in the regions where the aligned fibers are closest to the surface and are spaced apart where the transverse fibers are closest to the surface.

The total *V* deformation of the repeating unit increases with increasing temperature (Figs. 10 (a) and (c)), but the shape and distribution of the contours remain almost identical. Thus, inhomogeneity of the deformation along the fill direction does not change with relaxation of the matrix, within the temperature range of the creep tests.

Figure 11 presents contour plots for the *U* and *V* deformation of the repeating unit loaded along the warp direction at 27 and 70°C. As seen in the contour plots, the total *V*

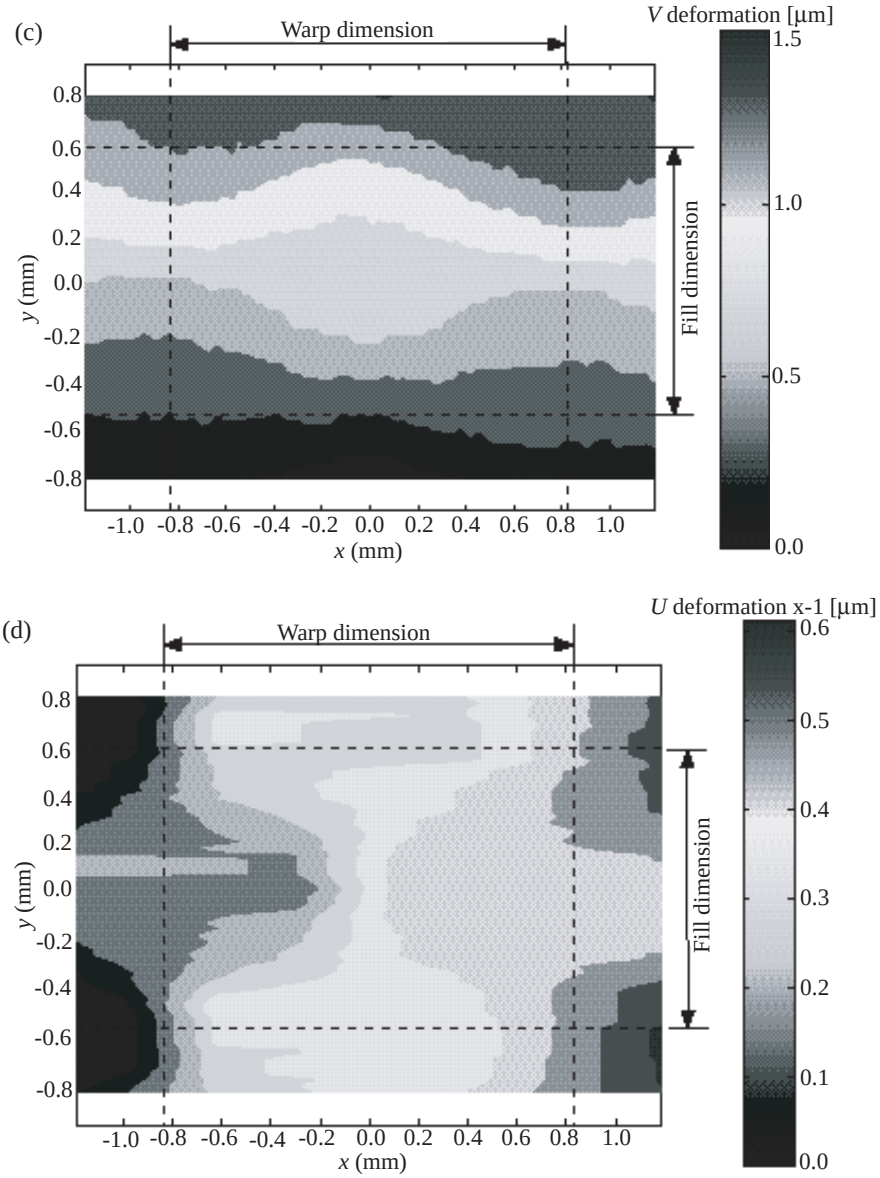

Fig. 10—(Continued from previous page)

deformation (Figs. 11 (a) and (c)) over the repeating unit (the difference between the top and bottom of the repeating unit) is nearly constant for any line drawn parallel to the loading direction. Similarly, the total *U* deformation (Figs. 11 (b) and (d)) at a given temperature is nearly constant for any line drawn perpendicular to the loading direction. The *V* and *U* deformations are symmetric about the centerline of the repeating unit. The symmetry is not readily observed for some plots, such as Fig. 11(d), because the deformation field includes the displacements due to rigid body rotation of the specimen.

The *V* and *U* deformations corresponding to warp direction loading follow the architecture of the repeating unit. The *V* deformation contours are close together in the center and corners of the repeating unit where the (fill) fibers aligned to the transverse direction are closest to the surface and are spaced apart at the mid-points of the edges where the longitudinal fibers are closest to the surface. Similarly, for the negative *U* deformation, the contours are spaced apart in the center and corners, and are close together at the mid-points of the edges.

The total *V* deformation in case of warp direction loading (Figs. 11 (a) and (c)) over the repeating unit increases with increasing temperature, indicating the relaxation of the composite. However, in contrast to the case of fill direction loading (Figs. 10 (a) and (c)), the shape and distribution of the contours also change with increasing temperature. At higher temperatures, the undulations of the individual contours decrease and the contour distribution becomes more uniform, indicating a decrease in the inhomogeneity of the displacement field along the warp direction.

The contour plots indicate that the deformation of the repeating unit is non-uniform, but offer no quantitative information about the degree of inhomogeneity. In order to obtain the

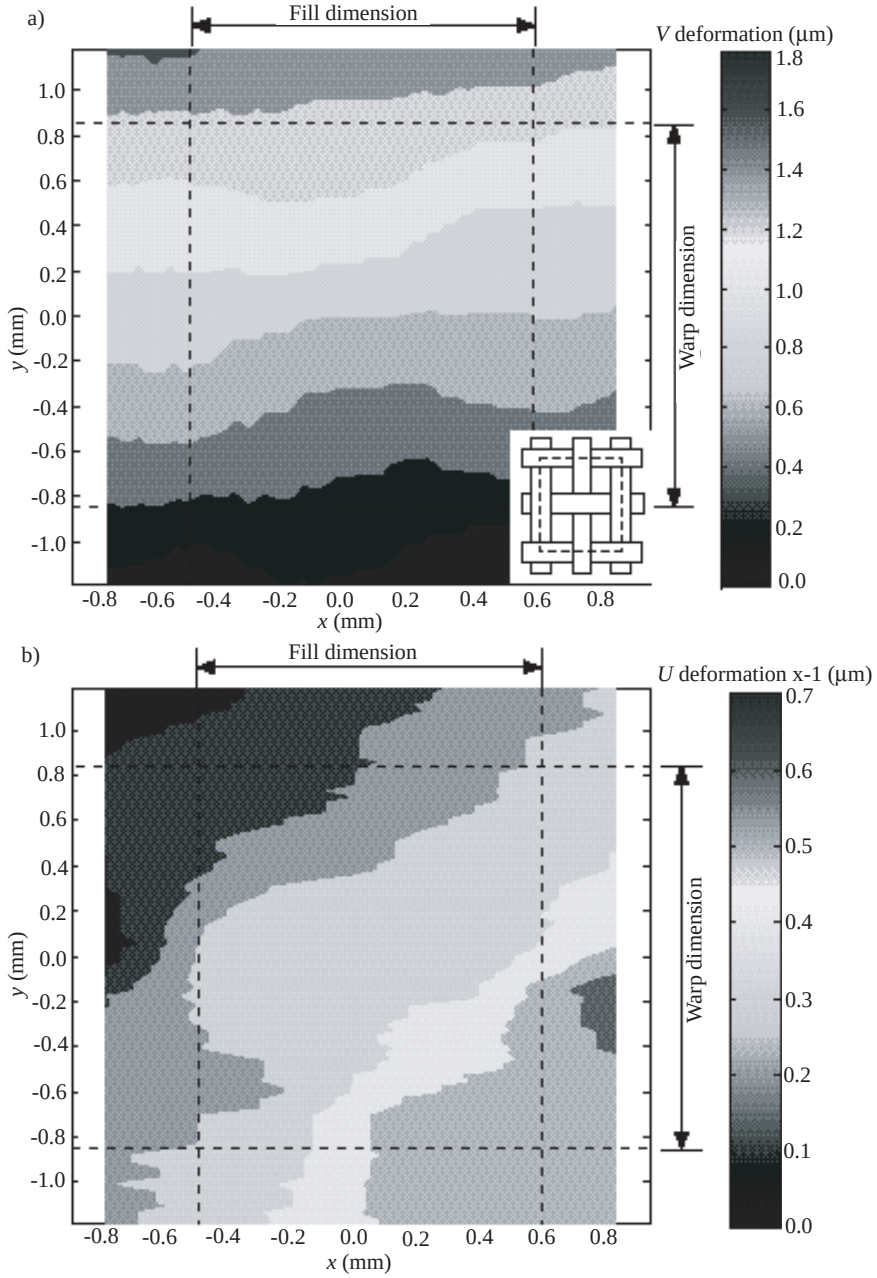

Fig. 11—Contour plot of displacement fields for the repeating unit loaded along warp direction: (a) V deformation at 27°C (architecture of repeating unit in the inset); (b) U deformation at 27°C; (c) V deformation at 70°C; (d) U deformation at 70°C
(Continued on next page)

tensile strain distribution over the repeating unit, the V deformation fields of the composite were differentiated along the loading direction. Strain variation over the repeating unit was determined by subtracting the average or nominal strain (see Fig. 8) from the calculated strain distribution. The resulting strain variation was further normalized by the corresponding nominal strain in order to highlight the strain inhomogeneity and to facilitate comparison between different temperatures and loading conditions. Contour plots of the normalized strain variation over the repeating unit for the different temperatures are presented in Fig. 12.

The strain variations in the repeating unit are clearly governed by the fabric architecture. The strain is approximately equal to the nominal strain in the regions where the fibers are located farther away from the surface and into the matrix. The regions of extreme magnitudes of strain occur at the locations where fibers are close to the surface, with maxima at locations where fibers are perpendicular to the loading direction and minima at locations where fibers are parallel. The strain variation is higher for loading in the fill direction (Figs. 12(a)–(d)) than in the warp direction (Figs. 12(e)–(h)), due to larger undulations (crimp angle, see Shrotriya and Sottos[5]) of the fibers.

For loading along the fill direction, the high strain regions are located at mid-points of the edges of the repeating unit at all four temperatures, with the highest strain being

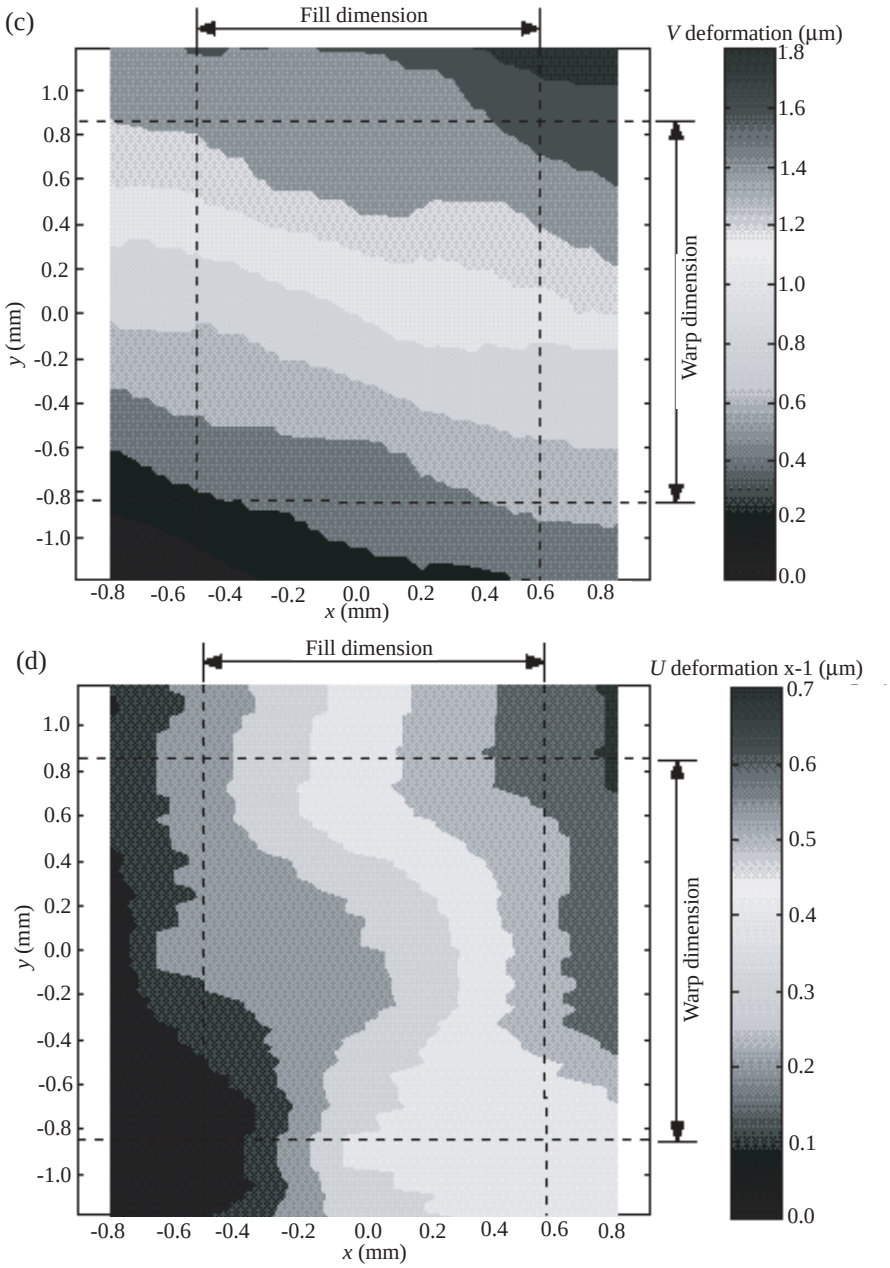

Fig. 11—(Continued from previous page)

approximately two times larger than the nominal strain. The low strain regions are located at the corners and the center, with the lowest strain being approximately half as large as the nominal strain. The order of regions of minima and maxima remains the same regardless of the temperature increase.

For loading along the warp direction, the high strain regions are located at the corners and in the center of the repeating unit at 27°C, with the highest strain approximately equal to 1.6 times the nominal strain. The low strain regions are located at the mid-points of the edges, with the lowest strain being about 0.6 times as large as the nominal strain. As the temperature is increased, the values for extrema remain the same, within the limits of experimental error, but the orders of regions of minima and maxima change significantly, particularly at the highest temperature. Such behavior could be due to the change of deformation mechanisms with increase in temperature. There may also be increased error associated with differentiation of the high-temperature deformation data.

Cross-Sectional Deformation

Deformation fields in the cross-section of the reinforcing fabric were obtained by testing the edge specimen discussed in the section on specimen preparation. The moiré images acquired during the creep test of fill direction specimens at 27°C are presented in Fig. 13, and those for the warp direction in Fig. 14. In addition, the images are compared with

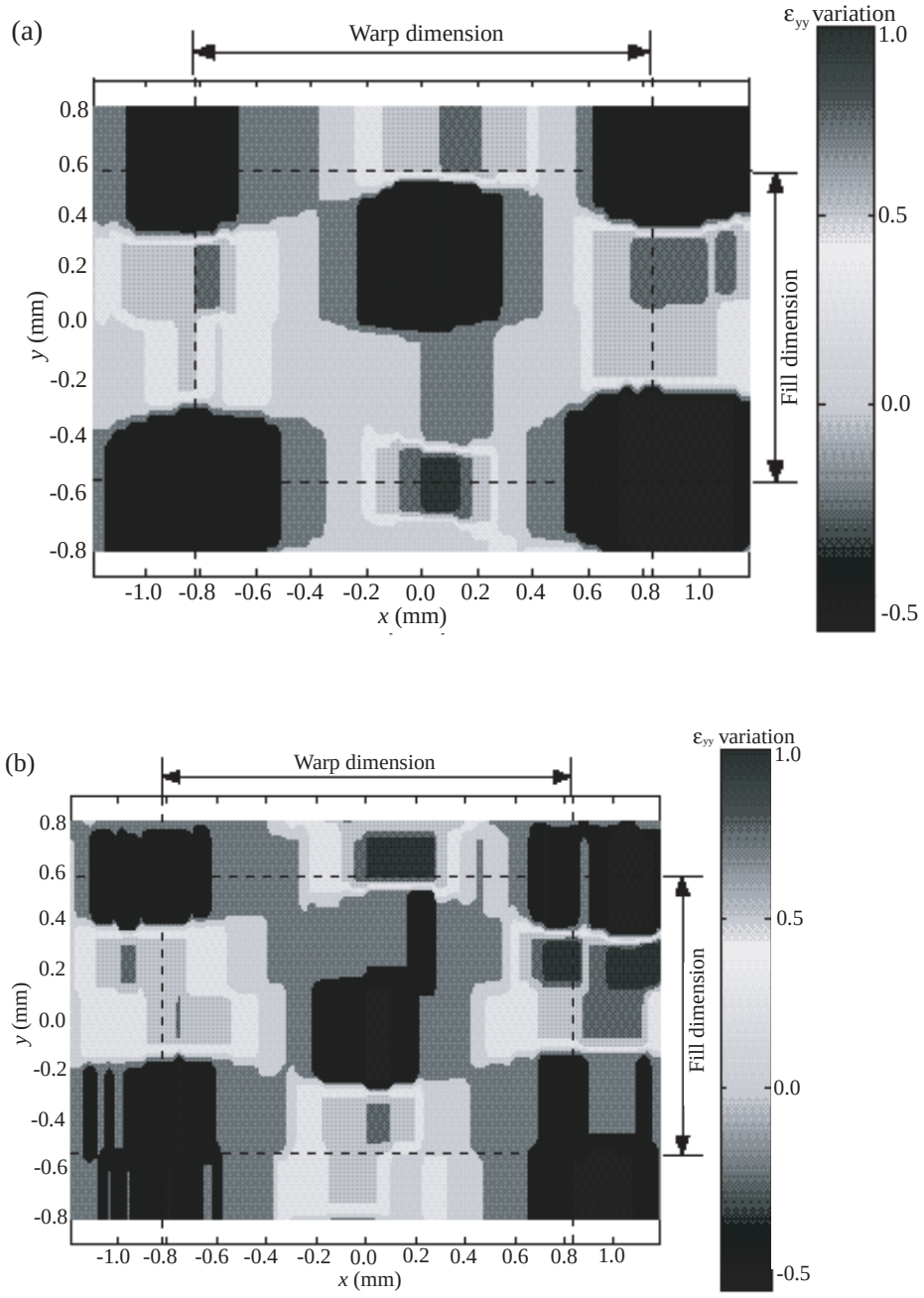

Fig. 12—Normal strain variation in the repeating unit: loaded along fill direction at (a) 27°C, (b) 40°C, (c) 60°C, (d) 70°C, and loaded along warp direction at (e) 27°C, (f) 40°C, (g) 60°C, (h) 70°C (continued on next page)

the optical micrographs of the composite in order to identify the unit cell. The transverse fiber bundles are sectioned and, consequently, the longitudinal bundles near the edge are relatively less constrained by the interlacing architecture than the bundles near the center. The distribution and structure of the fringes were used in order to ascertain the deformation mechanisms.

Moiré images corresponding to U and V displacements of both fill and warp direction specimens consist of periodically repeating fringe patterns. The fringe patterns are symmetric about their centerline and each half corresponds to a unit cell of the composite. The fringe pattern associated with the deformation along the fill direction is highlighted in Fig. 13 using lines A and C. One half of the similar fringe pattern associated with deformation along the warp direction is highlighted in Fig. 14 using lines A and B.

The fringe patterns in the unit cell are characteristic of deformation associated with bending loads and indicate that, even under uniaxial tensile load, the unit cell is subjected to localized flexural loading. Bending moments in the unit cell develop due to the undulations of fibers aligned in the loading direction. Furthermore, the symmetric nature of the pattern

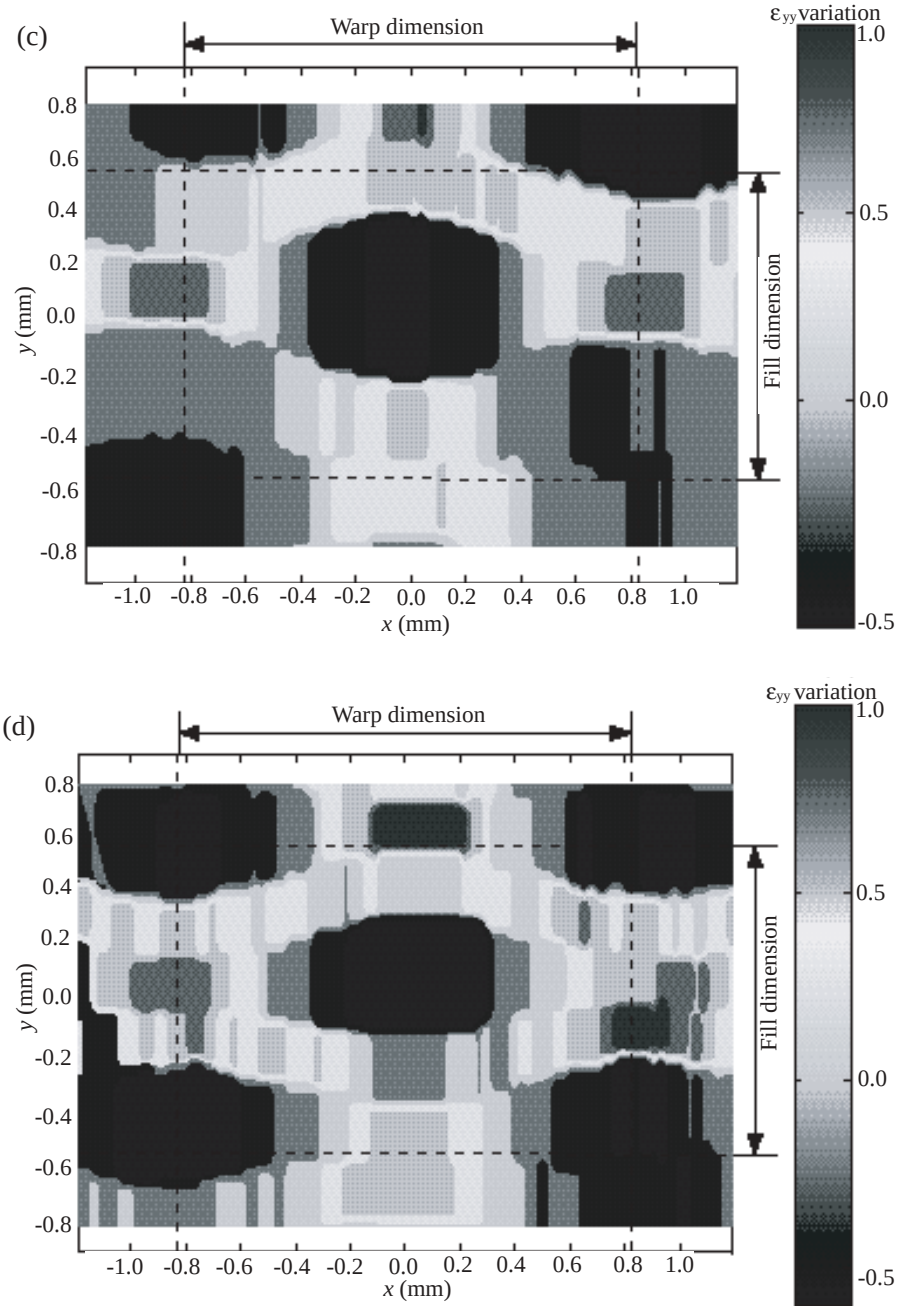

Fig. 12—(Continued from previous page)

indicates that the neighboring unit cells are subjected to equal and opposite bending moments. Therefore, the total bending moment over the repeating pattern is zero in accordance with the moment equilibrium for the whole specimen.

The images acquired at t = 600 s during the creep tests at different temperatures for both fill and warp direction specimens are presented in Figs. 15(a) and (b), respectively. In the images for both warp and fill direction specimens, the number of fringes in the periodic pattern increases with increasing temperature, indicating the increase in total deformation due to relaxation of the composite. In addition, there are no discernable changes in the shape and distribution of the fringes, suggesting that the deformation mechanisms do not change with the relaxation of the matrix, within the time and temperature range of the tests.

The fringe patterns associated with flexural deformation are observed consistently in all the images acquired during creep tests of both fill and warp direction specimens. The patterns corresponding to the warp direction specimens are sparse in comparison with those for the fill direction due to the combined effect of lower crimp angle and higher volume fraction of fibers aligned along the warp direction.

Discussion

Moiré interferometry reveals the influence of the fabric architecture on the deformation of woven composite substrate.

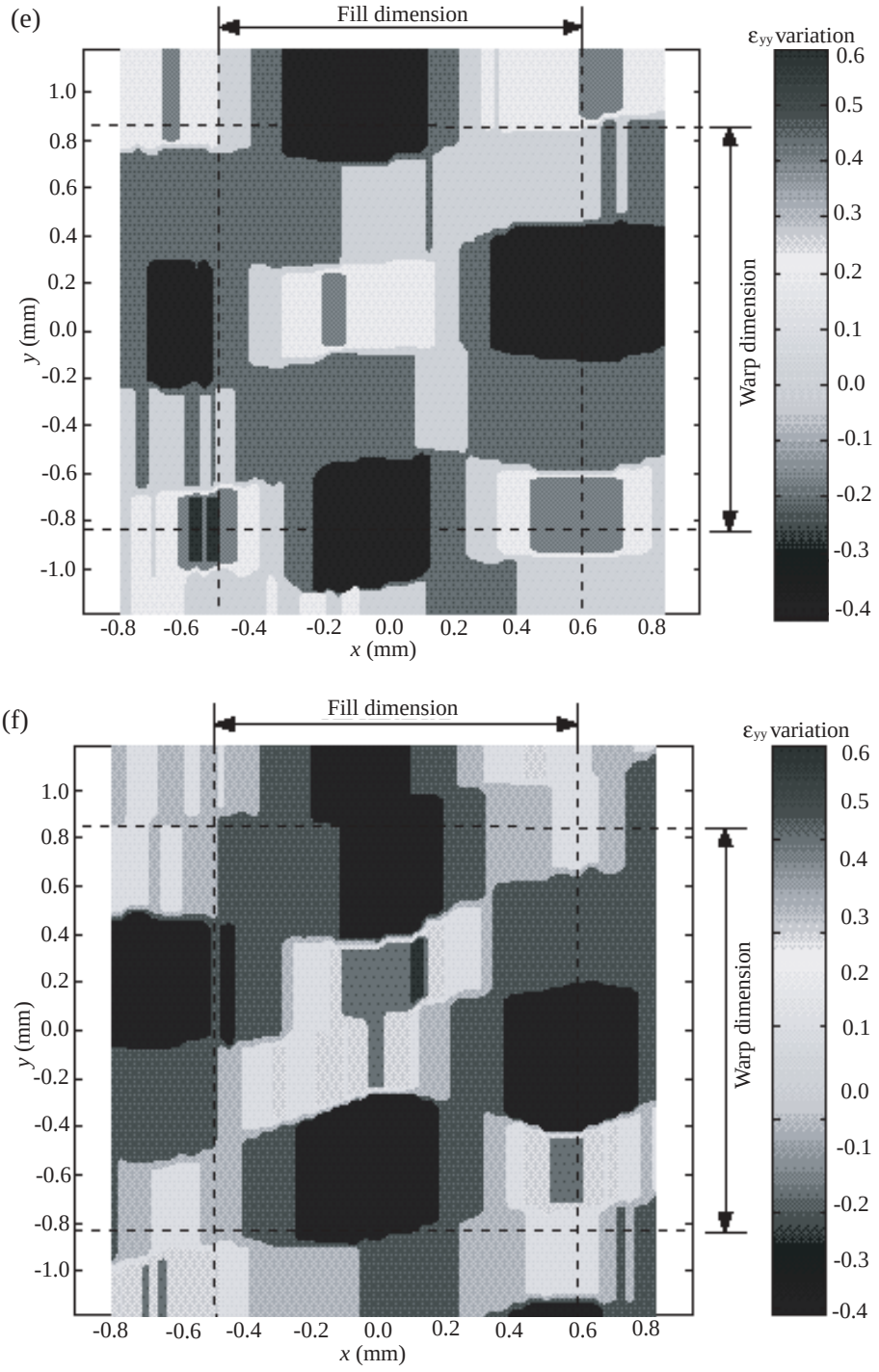

Fig. 12—(Continued from previous page)

Under the application of uniform tensile load, the in-plane deformation field over a unit cell of the composite is composed of a periodic pattern of alternating high and low fringe density regions (Fig. 10), and the cross-sectional deformation field displays fringe patterns similar to the bending deformation (Figs. 13 and 14). The magnitude of the local flexural deformation is determined by the crimp angle of the fiber bundles. For the 7628 fabric style, the fiber bundles along the warp direction have lower crimp angles compared to the bundles along the fill direction.[5] As a result, the strain variations over the repeating unit are higher for loading along the fill direction. For loading along the fill direction, the strain in the high strain regions is almost twice the nominal strain and is almost half the nominal strain in the low strain regions (Fig. 12(a)). Whereas, for loading along the warp direction the strain in high strain regions is 1.6 times the nominal strain and about 0.6 times the nominal strain in the low strain regions (Fig. 12(e)). The experimental results clearly indicate that the undulations of the fiber bundles lead to significant variations in the displacement field over the composite unit

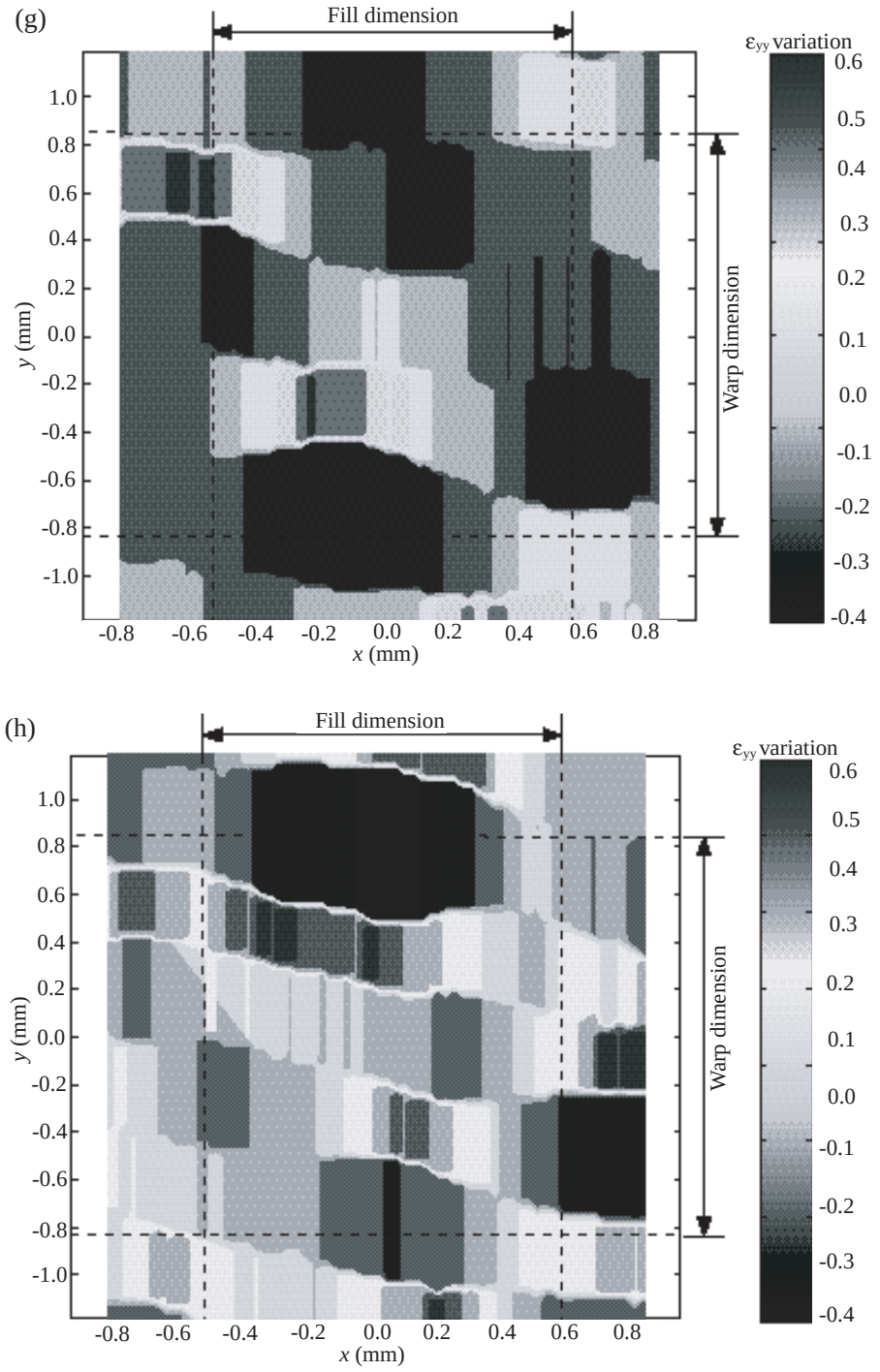

Fig. 12—(Continued from previous page)

cell due to localized flexural deformation. The variations in the strain and displacement fields indicate that local flexural deformation of the unit cell needs to be modeled for accurate predictions of woven composite properties. In addition, the local flexural deformation and corresponding strain variations will play a crucial role in determining the failure and damage mode of woven composites. Consequently, detailed investigations are required to study the influence of fabric architecture on the fatigue and fracture of woven composites.

The time–temperature-dependent response of the woven composite is anisotropic due to the differences in geometry and volume fractions of fiber bundles along the fill and the warp directions. In particular, the unrelaxed/elastic modulus along the warp direction is 1.2 times the modulus along the fill direction for the 7628 style woven composite (Table 1). Existing micromodels[1,5] can predict this difference in the moduli with good accuracy based on the constituents' properties and fabric architecture. The macro creep

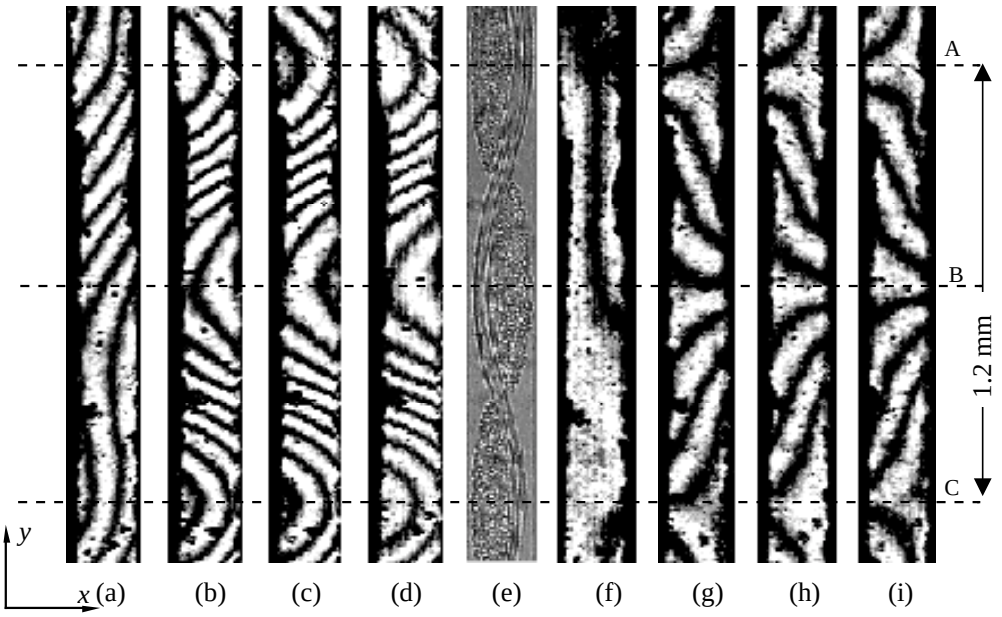

Fig. 13—Comparison of moiré images of fill direction specimen at 27°C with composite microstructure: (a) initial U field; (b) U field at $t = 0.1$ min; (c) U field at $t = 1$ min; (d) U field at $t = 10$ min; (e) composite microstructure; (f) initial V field; (g) V field at $t = 0.1$ min; (h) U field at $t = 1$ min; (i) V field at $t = 10$ min

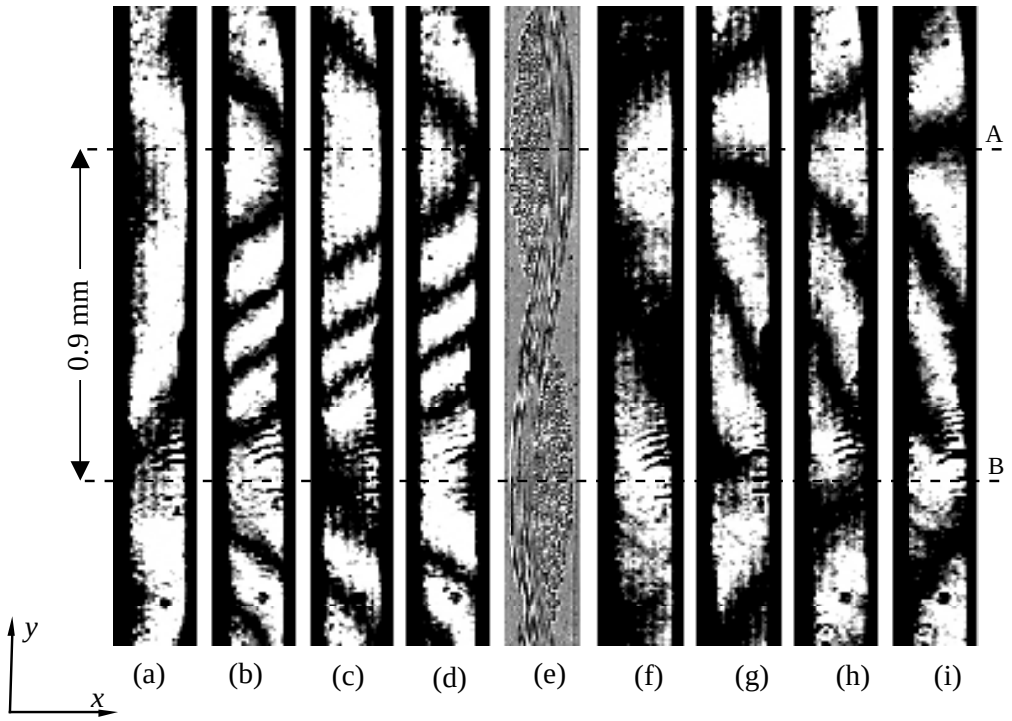

Fig. 14—Comparison of moiré images of warp direction specimen at 27°C with composite microstructure: (a) initial U field; (b) U field at $t = 0.1$ min; (c) U field at $t = 1$ min; (d) U field at $t = 10$ min; (e) composite microstructure; (f) initial V field; (g) V field at $t = 0.1$ min; (h) U field at $t = 1$ min; (i) V field at $t = 10$ min

(a)

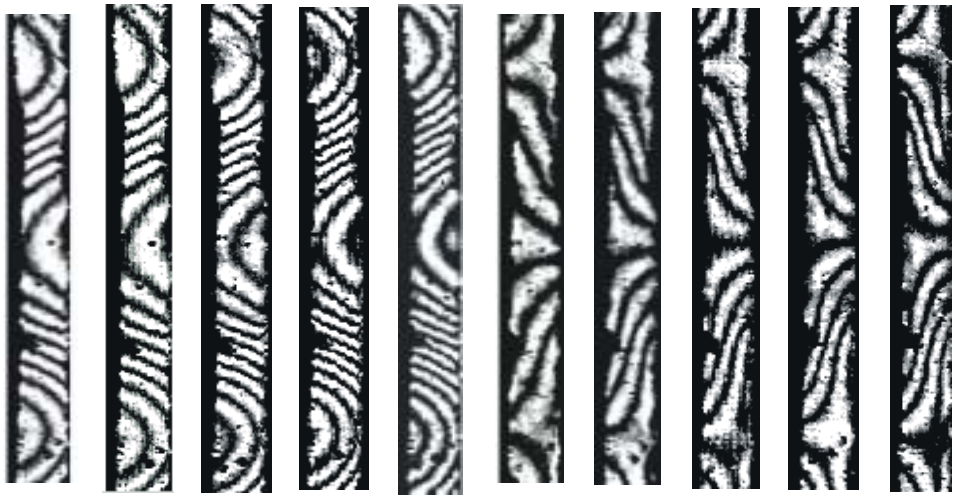

(1) (2) (3) (4) (5) (6) (7) (8) (9) (10)

(b)

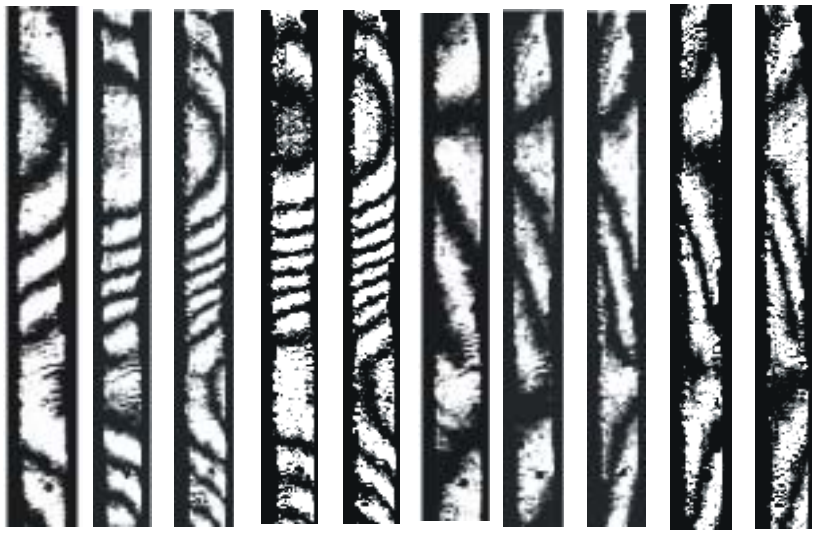

(1) (2) (3) (4) (5) (6) (7) (8) (9) (10)

Fig. 15—Moiré images of woven composite at different temperatures. (a) Fill direction specimen: (1) U field at t = 10 min and 27°C; (2) U field at t = 10 min and 40°C; (3) U field at t = 10 min and 60°C; (4) U field at t = 10 min and 70°C; (5) U field at t = 10 min and 80°C; (6) V field at t = 10 min and 27°C; (7) V field at t = 10 min and 40°C; (8) V field at t = 10 min and 60°C; (9) V field at t = 10 min and 70°C; (10)V field at t = 10 min and 80°C. (b) Warp direction specimen: (1) U field at t = 10 min and 27°C; (2) U field at t = 10 min and 40°C; (3) U field at t = 10 min and 60°C; (4) U field at t = 10 min and 70°C; (5) U field at t = 10 min and 80°C; (6) V field at t = 10 min and 27°C; (7) V field at t = 10 min and 40°C; (8) V field at t = 10 min and 60°C; (9) V field at t = 10 min and 70°C; (10) V field at t = 10 min and 80°C

experiments reported previously by Shrotriya and Sottos[5] and Wang et al.[4] have shown that the difference between the warp and fill responses becomes even more significant at higher temperatures and longer times. In fact, the fully relaxed modulus along the warp direction is almost 1.9 times the modulus along the fill direction for the 7628 style composite.[5] The measurements of the temperature-dependent in-plane deformation fields over the unit cell reported in this paper help explain the significant differences in macroscale relaxation behavior along the warp and fill directions. For the loading along the warp direction (Figs. 12(e)–(h)), the values for extrema remain the same with increase in temperature, but the order of regions of minima and maxima change significantly, particularly at the highest temperature. In contrast, for loading along the fill direction, the periodic pattern as well as the values of high and low strain regions are preserved with increase in temperature (Figs. 12(a)–(d)). Such behavior suggests a change of deformation mechanisms for loading along the warp direction with increase in temperature and, consequently, different relaxation behavior for loading along the warp and fill directions.

The results of current experiments provide both supporting and validation data for analytical models as well as finite element simulations of relaxation/creep behavior in woven composite. The experimentally measured local deformation fields reported in this paper can be utilized as a benchmark for comparison with model predictions in order to verify the physical basis of modeling assumptions. Shrotriya[13] performed a two-dimensional finite element simulation of the creep response of woven composite and compared the calculated displacement fields with moiré images of cross-sectional deformation field in order to verify that the finite element analysis model captured the low-temperature deformation mechanism of the composite. Similarly, Zhu et al.[14] have performed three-dimensional finite element simulations to determine the viscoelastic response of woven composite and compared the calculated displacement fields with the measured in-plane and cross-sectional deformations in order to verify the validity of the finite element analysis.

Conclusions

Moiré interferometry was utilized to visualize the in-plane and cross-sectional deformation fields of a unit cell of a woven composite substrate. The creep compliance, unrelaxed modulus, and the Poisson ratio determined using the moiré images, were in agreement with previous measurements. The deformation fields in the plane of the composite for loading along both the warp and fill directions consist of a periodic arrangement of high strain and low strain regions in accordance to the interlacing bundle architecture. The inhomogeneity of the deformation field was further demonstrated using contour plots of strain variations over the smallest repeating unit of the moiré images. The strain variations were higher for loading in the fill direction due to higher crimp angle of the fibers.

The deformation fields over the cross-section of the composite indicate that neighboring unit cells were subjected to equal and opposite bending moment even when the composite was loaded in uniaxial tension. Comparison of the unit cell deformation indicates that the unit cells along the fill direction deform more than those along the warp direction due to higher crimp angle and lower volume fraction of glass fibers.

The total deformation of the composite increased with increasing temperature, but the shape and distribution of the moiré fringes remained almost identical for all the loading cases and sample configurations. Therefore, the deformation mechanisms of the composite did not change with the relaxation of the matrix, within the temperature range of the experiments. The creep experiments demonstrate that moiré interferometry is an effective tool for investigating the nonuniform deformation of the woven composite.

References

1. Sottos, N.R., Ockers, J.M., and Swindeman, M., "Thermoelastic Properties of Plain Weave Composites for Multilayer Circuit Board Applications," Journal of Electronic Packaging, **121**, *37–43 (1999).*

2. Wu, T.Y., Guo, Y., and Chen, W.T., "Thermal–Mechanical Strain Characterization for Printed Wiring Boards," IBM Journal of Research and Development, **37**, *621–634 (1993).*

3. Yuan, J. and Falanga, L.A., "The In-Plane Thermal Expansion of Glass Fabric Reinforced Epoxy Laminates," Journal of Reinforced Plastics and Composites, **12**, *489 –496 (1993).*

4. Wang, T.M., Daniel, I.M., and Gotro, J.T., "Thermoviscoelastic Analysis of Residual Stresses and Warpage in Composite Laminates," Journal of Composite Materials, **26**, *883 –899 (1992).*

5. Shrotriya, P. and Sottos, N.R., "Creep and Relaxation Behavior of Woven Glass/Epoxy Substrates for Multilayer Circuit Board Applications," Polymer Composites, **19**, *567–578 (1998).*

6. Kuhn, J.L. and Charalambides, P.G., "Elastic Response of Porous Matrix Plain Weave Fabric Composites. I. Modeling," Journal of Composite Materials, **32**, *1426–1471 (1998).*

7. Kuhn, J.L. and Charalambides, P.G., "Elastic Response of Porous Matrix Plain Weave Fabric Composites. II. Results," Journal of Composite Materials, **32**, *1472 –1507 (1998).*

8. Tan, P., Tong, L., and Steven, G.P., "Modelling for Predicting the Mechanical Properties of Textile Composites – A Review," Composites Part A, **28A**, *903 –922 (1997).*

9. MirZadeh, F. and Reifsnider, K.L., "Micro-Deformations in C3000/PMR15 Woven Composite," Journal of Composite Materials, **26**, *185–205 (1992).*

10. Post, D., Han, B., and Ifju, P.G., High Senstivity Moire, Springer-Verlag, New York (1994).

11. Ifju, P.G., Masters, J.E., and Jackson, W.C., "The Use of Moire Interferometry as an Aid to Standard Test-Method Development for Textile Composite Materials," Composites Science and Technology, **53**, *155–163 (1995).*

12. Stout, E.A., "Characterization of Electronic Packaging Using Moire Interferometry," Masters Thesis, Theoretical and Applied Mechanics Department, University of Illinois at Urbana-Champaign (1997).

13. Shrotriya, P., "Dimensional Stability of Multilayer Circuit Boards," PhD Dissertation, Department of Theoretical and Applied Mechanics, University of Illinois at Urbana-Champaign (2000).

14. Zhu, Q., Shrotriya, P., Geubelle, P.H., and Sottos, N.R., "Viscoelastic Response of a Woven Composite Substrate for Multilayer Circuit Board Applications," Composite Science and Technology, **63**, *1971–1983 (2003).*